On the link between the Amazonian forest properties and shallow cumulus cloud fields

Reuven H. Heiblum[1], Ilan Koren[1] and Graham Feingold[2]

Correspondence to: I. Koren (Ilan.Koren@weizmann.ac.il)

[1]Department of Earth and Planetary Sciences, Weizmann Institute, Rehovot 76100, Israel

[2]NOAA Earth System Research Laboratory (ESRL), Chemical Sciences Division, Boulder, Colorado 80305, USA

Abstract

During the dry season the Amazon forest is frequently covered by shallow cumulus clouds fields, referred to here as Forest Cumulus (FCu). These clouds are shown to be sensitive to landcover and exhibit a high level of spatial organization. In this study we use satellite data to perform a morphological classification and examine the link between FCu cloud field occurrence and the Enhanced Vegetation Index (EVI), which is commonly used as a measure for forest density and productivity. Although weaker than first order effects of meteorology and biomass burning, a clear positive linear relation between EVI (i.e. surface properties) and FCu field occurrence is seen over forest landcover, implying a strong coupling between forest surface fluxes and the cloud organization above. Over non-forest landcover the relationship between EVI and FCu occurrence is non-linear, showing a reduction of FCu for high EVI values. We find that forest to non-forest transition zones display a superposition of the two different landcover dependencies.

1. Introduction

During the Amazon dry season (austral winter months, June-September), the Inter-Tropical Convergence Zone (ITCZ) moves northward (reaches ~10^{o}N at mid August), while large scale subsidence associated with the South Atlantic Subtropical High (SASH) dominates the region (Nobre et al., 1998) and relatively stable meteorological conditions prevail. Under these conditions, organized fields of shallow cumulus (Cu) clouds form over and near the forest during the daytime hours when surface triggered convection is possible and the humidity near the canopy is high enough. The formation of these clouds has a clear diurnal cycle with a maximum during the afternoon.

A typical satellite image of these cloud fields can be seen in Fig. 1, taken on September 1st, 2011, 13:30 local time. The clouds form almost exclusively over land areas; i.e. clouds are absent above the Amazon River and its tributaries. One of the noticeable, although not exclusive, properties of these clouds is their tendency to organize in linear patterns (Fig. 2). They can often be considered analogous to cloud streets (Ramos da Silva et al., 2011), which are typically observed during cold air outbreaks over warmer oceanic waters (Brümmer, 1999). In this work these cloud fields are shown to be very sensitive to changes in the environmental conditions and therefore they can serve as a "laboratory" for studying the conditions in which they form. They are hereafter referred to as Forest Cumulus (FCu) fields (more details on the FCu are given in Sect. 2). Daytime FCu cloud fields similar to those seen in Figs. 1, 2 can be observed in several other locations around the globe such as central Africa during most of the year, or northeast America and Siberia during the boreal summer. The common denominator in all cases is their preferred formation over dense, large-scale forests during stable meteorological conditions, when formation of more developed clouds is suppressed.

Landcover change effects on clouds can be divided by temporal and spatial scales into short (immediate) or long term effects, or local to global spatial scales (Pielke Sr et al., 2011); here we will focus on the short term ones. The immediate effects of landcover changes are attributed to changes in the surface radiation budget (Betts, 2009). Different landcover types exhibit different albedo, surface roughness, moisture content, etc. (Bastable et al., 1993). Such changes affect the energy fluxes to the atmosphere, the partition of this energy to sensible and latent heat, and the turbulent

transfer of those fluxes to the atmosphere. Eventually, these changes influence the diurnal evolution of the atmospheric boundary layer (Betts, 2000). The latter study showed how vegetation resistance controls the boundary layer depth (with lowest resistances corresponding to the oceanic limit) and the partition between latent and sensible het fluxes. Hence, the evapotranspiration properties of the landcover vegetation are tightly linked to the dynamics of the boundary layer and the shallow Cu clouds, which commonly cap the boundary layer.

Deforested areas in the Amazon (either pasture or cropland) usually display higher sensible heat and lower latent heat fluxes in comparison with the forested areas, which in turn can enhance the growth of the boundary layer during the day and favor the formation of larger convective clouds (Fisch et al., 2004). Moreover, surface heterogeneities often result in local mesoscale breezes which can also affect low-level convergence patterns and cloud formation (Rabin et al., 1990;Souza et al., 2000).

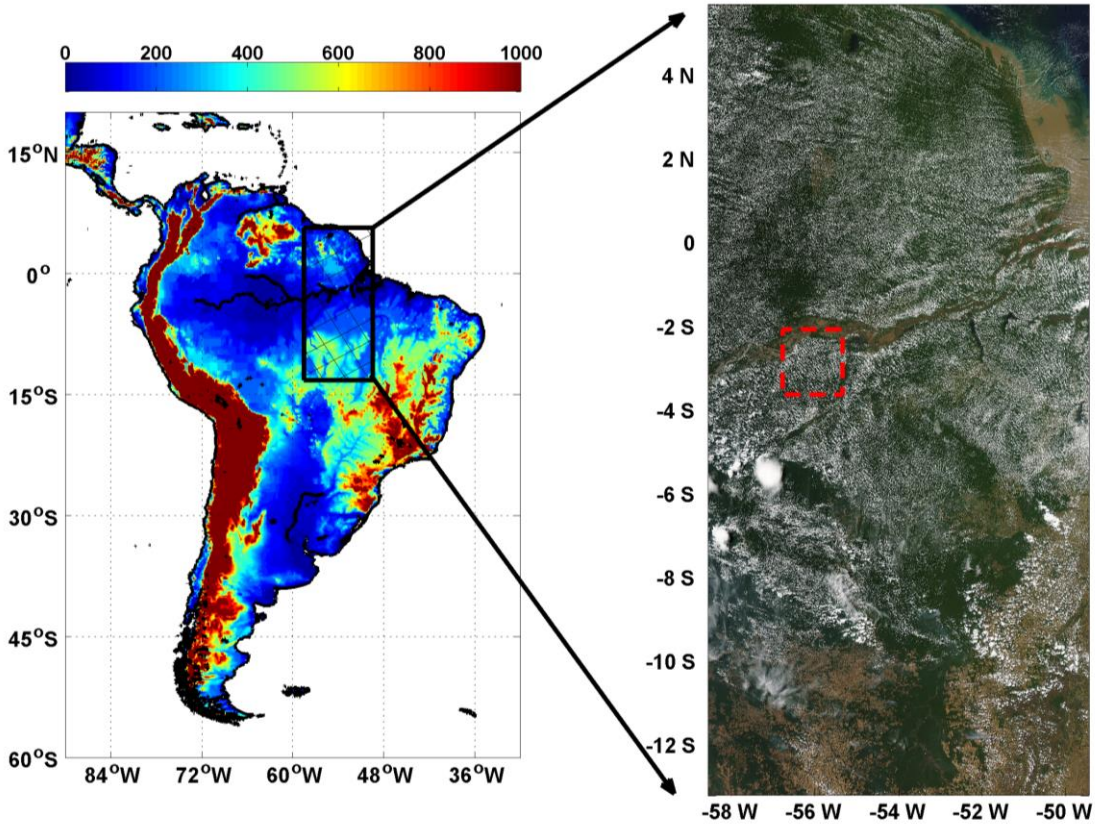

Figure 1. Left: South America topographic map (note that the color bar is capped at 1000 m) and study region indicated by cross hatched box. Map based on ETOPO1 1-arc minute global relief model dataset (Amante and Eakins, 2009). Right: Typical Forest Cumulus (FCu) fields over the Amazon basin study region. GeoTIFF image taken from MODIS Rapid Response USDA Foreign Agricultural Service (FAS)

subsets. Dashed red box indicates the area magnified in Fig. 2. Image corresponds to Sep. 1st, 2011, 13:30 local time. The Amazon River and its tributaries inhibit all types of cloud formation.

Generally there exists a preference for shallow Cu formation over densely forested rather than deforested areas (located around the southern boundaries of the Amazon basin, see Fig. 1) (Cutrim et al., 1995). However, most observational studies, including those listed above, have focused exclusively on deforested pockets within forested areas, showing a clear preference for shallow Cu formation over *deforested* areas (Cutrim et al., 1995;Chagnon et al., 2004;Wang et al., 2009), and for deep convective cloud formation over the surrounding forested areas (Wang et al., 2009). These differences in shallow Cu preference could arise since emphasis was put on the importance of mesoscale circulations driven by landcover transitions rather than more subtle changes within a specific landcover type. Moreover, studies showing preference for shallow Cu over deforested landcover are confined mainly to the southwest regions of the Amazon, which are highly deforested and experience very stable meteorological conditions during the dry season. Studies in other regions of the world such as southwest Australia (Ray et al., 2003) and Costa-Rica (Nair et al., 2003) show a preference for shallow cumulus formation over native vegetation and forested areas rather than adjacent deforested areas.

Figure 2. Magnified view of Forest Cumulus (FCu) cloud fields (subset of Fig. 1). Note the linear patterns in which the FCu organize. The scale of the box is 150 km x 175 km.

Much of the Amazon deforestation is a result of massive biomass burning events which occur during the dry season (Koren et al., 2004). Biomass burning emits high concentrations of absorbing aerosols to the atmosphere, which can interact with radiation (i.e. scatter and absorb shortwave radiation) and affect the temperature profile and therefore static stability, or serve as Cloud Condensation Nuclei (CCN) and affect the microphysical processes and evolution of clouds and precipitation (Koren et al., 2008). Hence, it is essential to address aerosol effects on clouds and to try to distinguish them from the landcover change effects on clouds.

The goal of this work is to evaluate the morphological characteristics of the Amazon FCu fields, and to use a statistical approach to study the effects of landcover change on the FCu fields over the Amazon region. Specifically we use the EVI (Enhanced Vegetation Index) as a measure of the wellbeing of the forest. It has been shown that this index correlates well with forest productivity and canopy density, and can be a

good predictor for evapotranspiration and moisture fluxes to the lower atmosphere, which in turn drive the formation of Amazonian clouds.

2. Methods

We combine satellite data in the visible for cloud morphology and Aerosol Optical Depth (AOD) analyses, landcover type and vegetation indices for surface characterization, and reanalysis data for specification of the meteorological conditions. True color data at 0.5 km resolution, AOD data at 1^0 resolution, and land surface properties derived from the MODerate resolution Imaging Spectroradiometer (MODIS) onboard the Aqua satellite are used (Salomonson et al., 1989;Friedl et al., 2010;Running et al., 1994;Remer et al., 2005). The Aqua overpass is at 13:30 LST, at the time when energy fluxes from the surface are maximum (Fisch et al., 1996) and the FCu fields over the Amazon are already established. The study region of interest is seen in Fig. 1, and spans from 58.54^{o}W, 5.69^{o}N (northwest corner) to 49.45^{o}W, 13.19^{o}S (southeast corner), an area of 2100 km x 950 km. The topography of the study region is low, and devoid of large gradients except some patches in the northern part, and a gradual rise to higher topography in the southern part. Analyses show that the FCu fields had no clear correlation with topography. Therefore, we exclude analyses of topography effects in this work. Data were collected for the dry season months, July-August-September (J-A-S) during the years 2008-2011.

Our analyses of the FCu cloud field properties were focused on the statistical properties of the cloud distribution within the field. Measures like cloud area, average distances between cloud centers and level of organization were tested to optimize the classification. Unlike the case of a single cloud analysis when the sensitivity to the exact cloudy pixel is crucial and one need either to avoid cloud contamination of the cloud–free atmosphere (Martins et al., 2002), or in the case of cloud retrievals to make sure that the cloud mask is free of non cloudy pixels (Ackerman et al., 1998), our spatial-statistical measures (summarized in Fig. 3) exhibit less sensitivity to the exact method by which clouds are masked in the field.

The first stage of processing is a construction of a basic cloud mask, achieved by applying a threshold (>0.58) to the reflectance of the RGB channels (bands 1, 3, 4, respectively). Unlike clouds, most bright pixels that are not clouds (e.g. bright roads

or sand patches) are not white (e.g. have spectral dependence in the visible spectrum) therefore another threshold (<0.08) is applied to the absolute differences in the reflectance between the red and blue. The morphological characteristics of the cloud field were calculated for a moving window of 51 x 51 pixels (25.5 km x 25.5 km). Five basic characteristics were shown to contain most of the information: cloud fraction, mean and standard deviation of distances between cloud centroids, and mean and standard deviation of cloud areas.

Based on the above criteria we classified the cloud fields into three classes: FCu, deeper convective clouds and sparse to no-clouds (see Table 1). The classification was tuned and validated visually using data from 100s of boxes of cloud fields (see Fig. 3c). The boxes were used to calculate the mean statistics of the FCu clouds fields. The typical values for the morphological characteristics of the three defined fields types are shown in Table 2. The narrow distributions and inter-annual consistency of these key cloud properties allowed for a robust detection of the fields.

After performing the analysis above for all days during J-A-S for a specific year (a total of 75-80 overpasses), the probability for an FCu field to exist (hereafter named pFCu) was calculated for each pixel (see Fig. 3d). Similar methodologies have been used in other studies of shallow cumulus clouds (Ray et al., 2003;Cutrim et al., 1995). It is important to note that the classification results were shown to be robust and not sensitive to small variations in the selected thresholds.

Yearly classification of different landcover types was done using the MODIS collection 5 MCD12Q1 product (Friedl et al., 2010). The product includes five types of landcover classifications, out of which the 14-class University of Maryland (UMD) classification was chosen (Hansen et al., 2000). For the purposes of this study, we divided the UMD landcover classification into three types: i) Forest, classes 1 through 5 (i.e. all forest types including mixed), ii) Non-Forest, classes 6 through 10 (wood-lands, grasses, shrub-lands), 12 (crop-lands), 13 (urban), and 16 (barren), and iii) Water, class 17. An example of such a classifcation map for 2011 is seen in Fig. 4a.

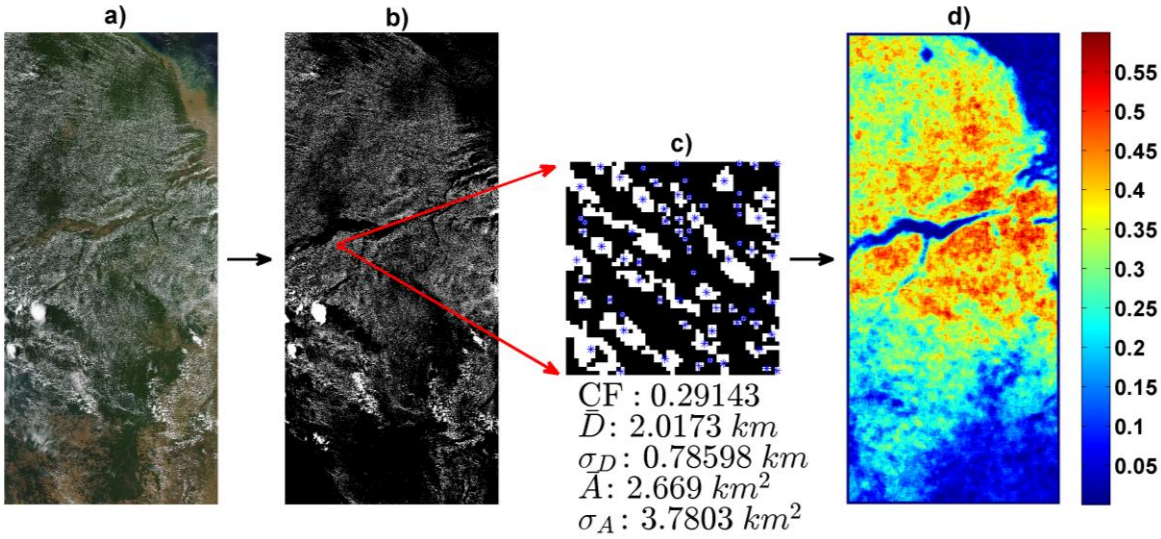

Figure 3. Summary of FCu field detection algorithm for 2011. a) Corresponding true color geoTIFF image from Fig. 1. b) Cloud mask of true color image; the red box represents a 25.5 km x 25.5 km moving window. c) Zoom of the moving window. Blue asterisks indicate the centroids of individual clouds. Selected statistics of windows are listed below the panel. In this case the cloud field within the window passed the FCu field thresholds listed in Table 1. d) Final product of algorithm, probability (0-1) of observing FCu field (pFCu) during J-A-S 2011.

Spectral definitions for MODIS vegetation indices: NDVI (Normalized Difference Vegetation Index) and EVI (Enhanced Vegetation Index), and their validations over numerous sites can be found in previous papers (Huete et al., 2002;Mu et al., 2007). Both vegetation indices can be used to assess the surface energy budget components (latent heat, Bowen ratio) and plant physiology components such as evapotranspiration, leaf area index, fractional vegetation cover, canopy architecture and more (Glenn et al., 2008). Since NDVI tends to saturate in areas of high biomass (Huete et al., 2002), and is more sensitive to atmospheric aerosol contamination (Xiao et al., 2003), EVI is preferred in our study.

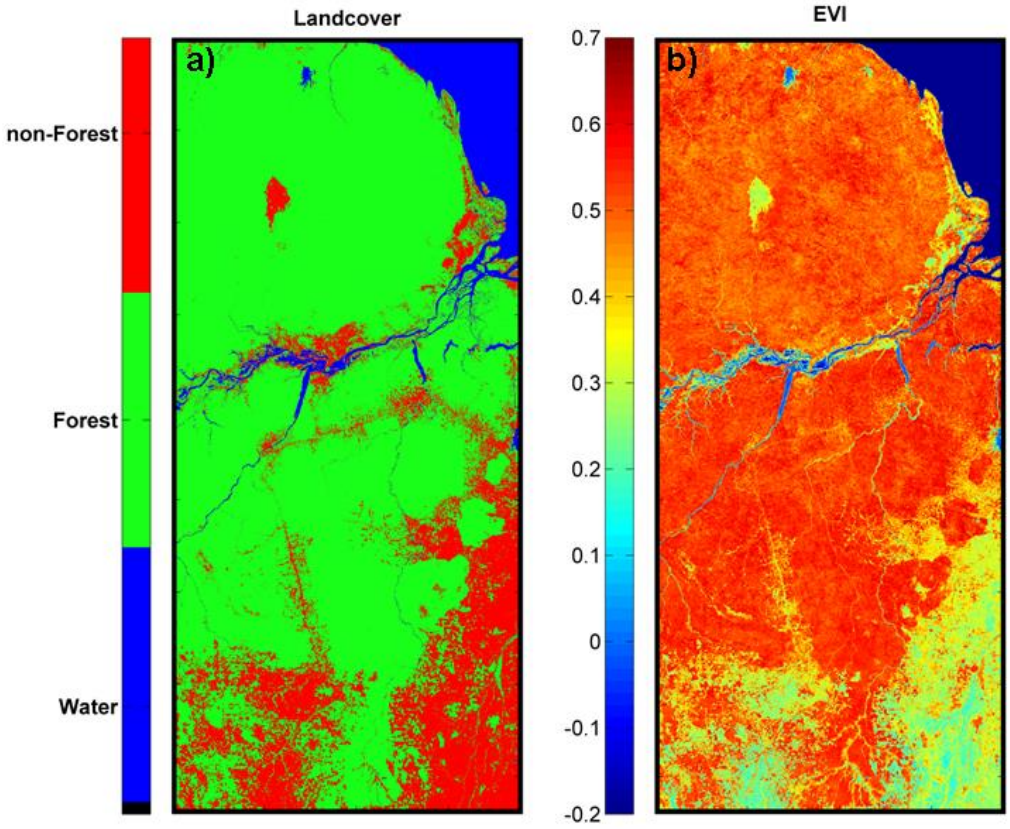

Figure 4. Landcover classification map (a) and mean J-A-S EVI (b) for the year 2011.

Furthermore, studies have shown EVI to be better correlated with evapotranspiration than NDVI, with linear correlation coefficients (r^2) usually ranging between 0.7 and 0.9 (Glenn et al., 2010;Nagler et al., 2005). Henceforth we shall use EVI as a general measure of vegetation density and productivity over the forest and non-forest landcovers. The mean J-A-S EVI for 2011 is shown in Fig. 4b. The domain shows high EVI values over forest landcover in comparison with non-forest landcover, with the latter also showing much larger EVI variance. Very similar EVI maps are seen for years 2008-2010.

Focusing on the southern half of the domain, Fig. 3d clearly shows reduction in the probability for FCu fields. The same pattern exists for the year 2008-2010. Using NOAA-NCEP Global Data Assimilation System (GDAS) reanalysis data (Saha et al., 2006;Parrish and Derber, 1992), we examined the spatial patterns of various meteorological parameters (J-A-S averages). The two parameters that were found to best reflect the spatial variance of the FCu fields are the Geopotential Height (HGT) at 700 hPa (see Fig. 5a) and the Relative Humidity (RH) at 850 hPa (see Fig. 5b).

These parameters can also be seen as physically tightly linked to FCu formation. High geopotential height at 700 hPa (pressure levels 850 hPa – 500 hPa give similar results) indicates upper level subsidence, adiabatic warming and drying, and is associated with the SASH (Figueroa and Nobre, 1990). Relative humidity at 850 hPa corresponds to the mean cloud base height (based on ceilometer measurements), and is essential to cumulus formation.

Table 1. Moving window thresholds for Forest Cu (FCu), Deep Convective Cu, and none to sparse Cu cloud fields. Thresholds include cloud fraction (CF), mean cloud area ($\bar{A}$), standard deviation of cloud areas (σ_A), mean distance between cloud centroids ($\bar{D}$), and standard deviation of distances (σ_D). Missing data represent thresholds that are not relevant to the analysis.

Parameter →	**CF [%]**		**$\bar{A}$ [km^2]**		**σ_A [km^2]**		**$\bar{D}$ [km]**		**σ_D [km]**	
Field Type↓	**Low**	**High**	**Low**	**High**	**Low**	**High**	**Low**	**High**	**Low**	**High**
Forest Cumulus	0.15	0.4	1.5	8	1.5	12.5	1.8	3.2	0.6	1.3
Sparse	0	0.1	0	3	0	3	-	-	-	-
Deep Convective	0.6	1	50	-	-	-	-	-	-	-

Table 2. Average statistics for the cloud fields (and their spatial parameters) as defined in Table 1, years 2008-2011. Missing data represents irrelevant statistics (e.g. distance between clouds is meaningless for sparse and deep convective fields since we commonly observe only one cloud within the 25 km moving window).

Parameter → **Field Type↓**	**Year**	**CF [%]**	**$\bar{A}$ [km^2]**	**σ_A [km^2]**	**$\bar{D}$ [km]**	**σ_D [km]**
Forest Cumulus (FCu)	2008	0.23±0.02	2.93±0.37	5.79±1.08	2.21±0.12	0.91±0.07
	2009	0.23±0.02	3.00±0.31	5.64±0.95	2.26±0.10	0.90±0.06
	2010	0.24±0.02	3.03±0.41	5.80±1.13	2.25±0.13	0.88±0.07
	2011	0.24±0.02	3.13±0.37	5.65±1.00	2.31±0.13	0.87±0.07
Sparse	2008	0.03±0.02	1.31±0.43	1.33±0.43	-	-
	2009	0.04±0.01	1.24±0.38	1.24±0.42	-	-
	2010	0.03±0.02	1.55±0.62	1.54±0.63	-	-
	2011	0.03±0.02	1.39±0.47	1.33±0.50	-	-

Deep Convective	2008	0.83±0.06	144.0±58.2	-	-	-
	2009	0.82±0.06	139.7±56.7	-	-	-
	2010	0.83±0.06	143.5±56.4	-	-	-
	2011	0.83±0.06	143.9±59.8	-	-	-

3. Results

3.1. Forest Cumulus (FCu) dependence on meteorology

The meteorological context of the FCu probability for 2011 is shown in Fig. 5c and d. The north-south pFCu differences over the land are best captured by the Geopotential Height (HGT) at 700 hPa field. The value of HGT=3157 meters (indicated by the dashed line in Fig. 5a and solid line in Fig. 5c) was chosen as the boundary between the northern part of the Amazon region (NA in Fig. 5a,c) that shows little meteorological variance and the southern part of the Amazon region (SA in Fig. 5a,c) that shows high coupling between pFCu and meteorology. Hence, in order to minimize meteorological influence, only the northern region (NA) is used to test large-scale vegetation index effects on FCu fields.

Patterns of RH at 850 hPa may affect some of the features seen in Fig. 3d as well. The southeast to northwest positive gradient in the southern Amazon (SA) pFCu seems to correspond to an equivalent RH gradient seen in Fig. 5b. Additionally, from the dependence of pFCu on RH in Fig. 5d we can see that areas with high RH (RH>80%, indicated by the dashed line in Fig. 5b) are less favorable for FCu formation. The high RH areas are mainly coastal regions, and the reduction in pFCu there is probably due to increased cloud activity (i.e. the cloud fraction (CF)/mean area (σ_A) in coastal areas is frequently above the upper thresholds in Table 1) as a result of mesoscale coastal breezes observed in many previous works (e.g.,(Heiblum et al., 2011;Malda et al., 2007)).

As seen in Fig. 5c,d, the large scale pFCu dependence on the two meteorological parameters is similar for both forest and non-forest landcover types.

Meteorological dependencies of EVI were checked as well for both forest and non-forest landcovers. For the forest landcover (as can be seen in Fig. 4), EVI is relatively constant for all meteorology, indicating that EVI reflects an inherent forest property. However, the non-forest landcover EVI is tightly linked to the meteorology, and

therefore any correlations between EVI and pFCu over non-forest may actually correspond to meteorological variance.

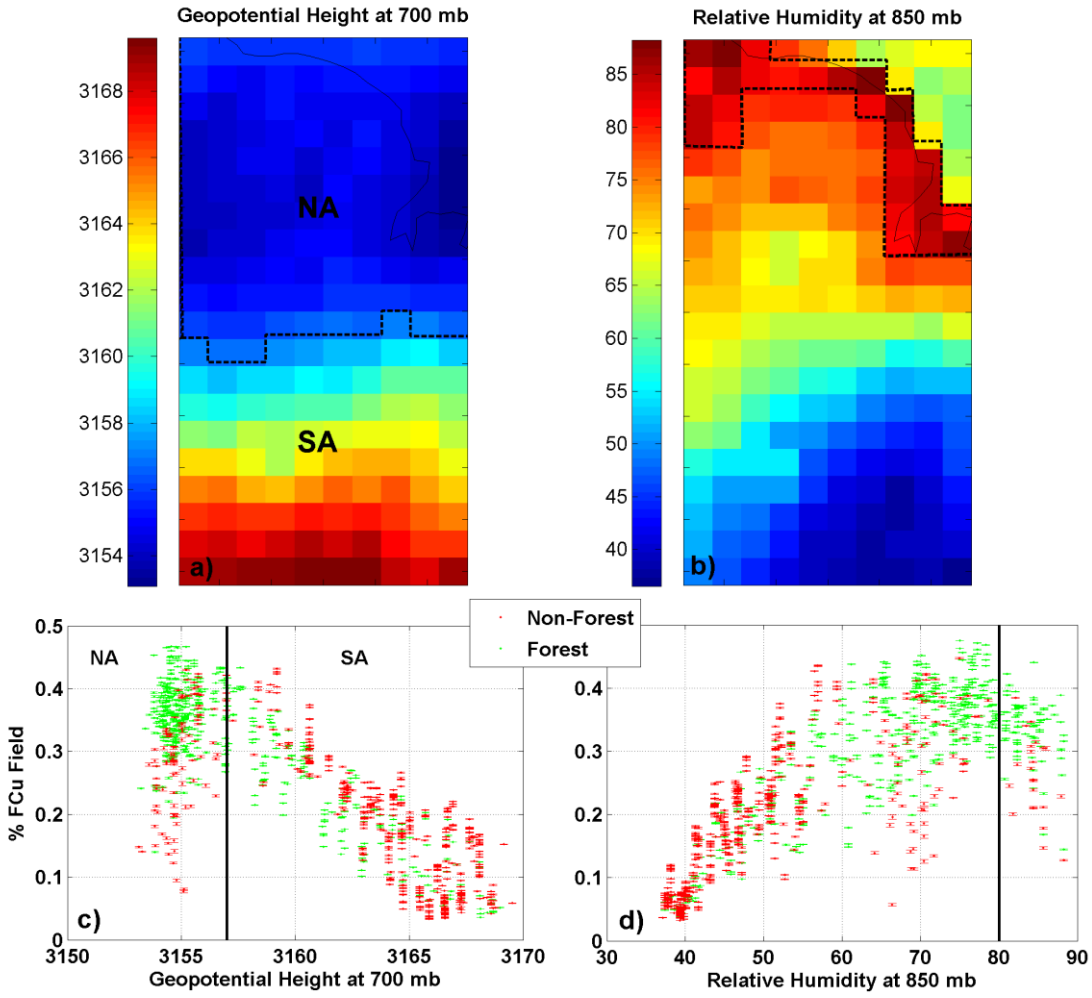

Figure 5. Meteorological setting (based on GDAS reanalysis data) in the Amazon during J-A-S and the effects on pFCu over forest and non-forest landcovers. a) Geopotential Height (HGT) [m] at 700 hPa pressure level; the dashed line represents the border between NA and SA regions. b) Relative Humidity (RH) [%] at 850 hPa; high RH areas enclosed within the dashed line are excluded from further analyses. c) Chance of observing FCu field as a function of HGT at 700 hPa. Data is sorted into 500 bins, 11484, 2808 counts per bin for forest and non-forest, respectively. Black line represents HGT separation between NA and SA regions. d) Same as ***c****, but for RH at 850 hPa. Data above RH=80% (black line in panel) is excluded from analyses in this work.*

3.2. Interannual Comparison of Cloud Fields and AOD

The average aerosol optical depth (AOD) together with the cloud field detection algorithm results for the years 2008-2011 are summarized in Fig. 6. Previously discussed cloud features such as FCu field preference over the northern part of region, and preference for deep convective clouds in high RH areas (i.e. coastal and northwestern areas) are seen for all four years. The relatively high chance for deep convective clouds in the northwest part of the study region may be due to variable terrain and complex topography in that region as well (see Fig. 1). Water bodies such as the Amazon River, Atlantic Ocean, and lakes clearly inhibit all types of cloud formation**.** The southern part of the region experiences little or no clouds at all, due to the dry and stable meteorology in that area. The year 2009 shows the highest occurrence of FCu formation throughout the domain. Meteorological conditions during that year show a more homogeneous pattern of RH at 850 hPa compared to other years (i.e. higher RH at the southern part (SA) and lower RH in the northern part (NA)), which could be responsible for increase in pFCu.

A striking difference in AOD between the years can be seen, with average values reaching above 0.4 (0.8) in the southwest part of the region during 2008 (2010) but limited to 0.25 during 2009 and 2011. Moreover, the spatial variance of AOD is much smaller during 2009 and 2011, and is unlikely to be a major factor in pFCu variability. The extremely high AOD during 2010 can be explained by both the extreme drought (Lewis et al., 2011) and frequent fires (Ten Hoeve et al., 2012) (i.e. abundance of biomass burning aerosol) in the Amazon basin that year. However, it should be noted that the drought's effect on our study region was minimal compared to the rest of the basin.

Although the general patterns of clouds field probabilities are similar for all years, the most significant differences appear to be related to AOD effects. Areas of high AOD (AOD > 0.5, indicated by white dashed contours in Fig. 5) during 2010 correspond to areas of lower pFCu and a higher probability of observing sparse or no-clouds in comparison with the other years. Moreover, the northern border of the high 2010 AOD plume acts as a boundary between low and high pFCu values. Although we also see elevated values of AOD during 2008, they are much lower and spatially localized in comparison with 2010, and we do not see the same reduction in FCu. The results for 2010 are consistent with previous findings in the Amazon (Koren et al.,

2004;Davidi et al., 2009). Shortwave radiation absorbed by biomass burning aerosols heats the mid-atmospheric levels, which results in stabilization of the atmospheric profile and reduction in cloud cover.

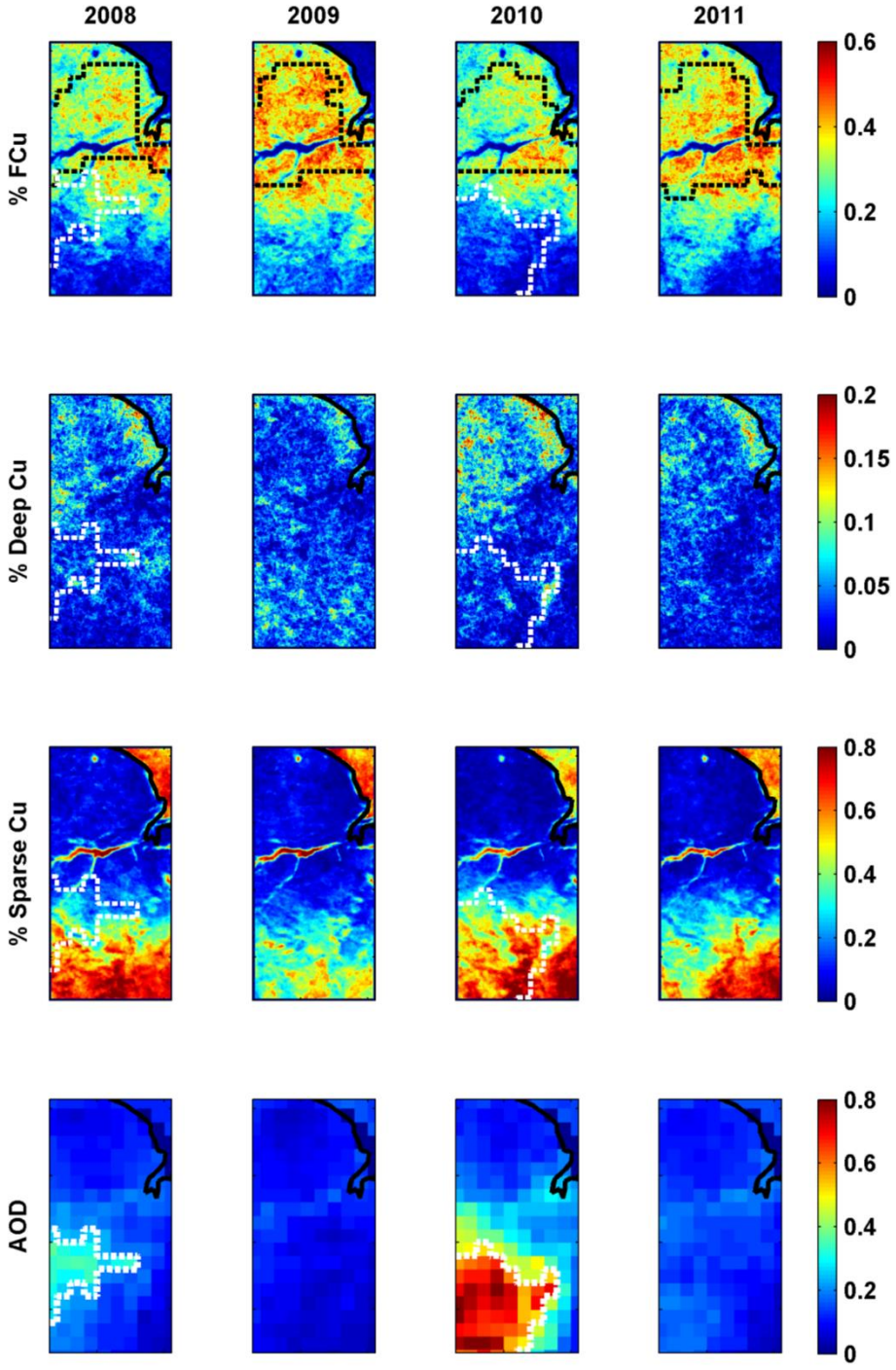

Figure 6. Cloud field statistics and AOD during J-A-S for 2008 (left panels) to 2011 (right panels). Panels include (from top to bottom) chance for FCu field, chance for deep convective cumulus field, chance for sparse to none cumulus field, and mean AOD taken from Giovanni online data system. White dashed contours in 2008 (2010)

panels indicate AOD>0.25 (0.5) region. Black dashed contours in upper panels represent areas with minimized meteorological variance (see Sect. 3.1), for each year, used in section 3.3 for EVI vs. pFCu analyses. The effects of high AOD during 2010 are apparent in all types of cloud fields, where the high AOD plume clearly inhibits FCu fields in southwest Amazon in comparison with other years. High AOD pixels along the mouth of the Amazon River were discarded as they correspond to a MODIS AOD algorithm artifact in that area due to the sediment-laden waters there.

To illustrate the potential effects of aerosols on FCu fields, we specifically compare the years 2010 and 2011. The relative difference between pFCu during 2010 and 2011 is shown in Fig. 7. We define the relative difference here as: $\frac{pFCu_{2011}-pFCu_{2010}}{\overline{pFCu}}$, where $\overline{pFCu}$ is the two year average. A low-pass 60 km radius filter was applied to reduce small-scale variability. Although pFCu was higher throughout most of the study region in 2011, the largest differences (up to 90%) are seen in areas of high AOD during 2010, whereas in other parts of the domain, relative differences are limited to the -15% to 50% range.

A comparison of the meteorological parameter averages between years 2010 and 2011 in the high AOD region shows minor differences of less than ±2 m for HGT at 700 hPa and 0%-10% for RH at 850 hPa, suggesting that the lower pFCu during 2010 was due to high AOD and not meteorology.

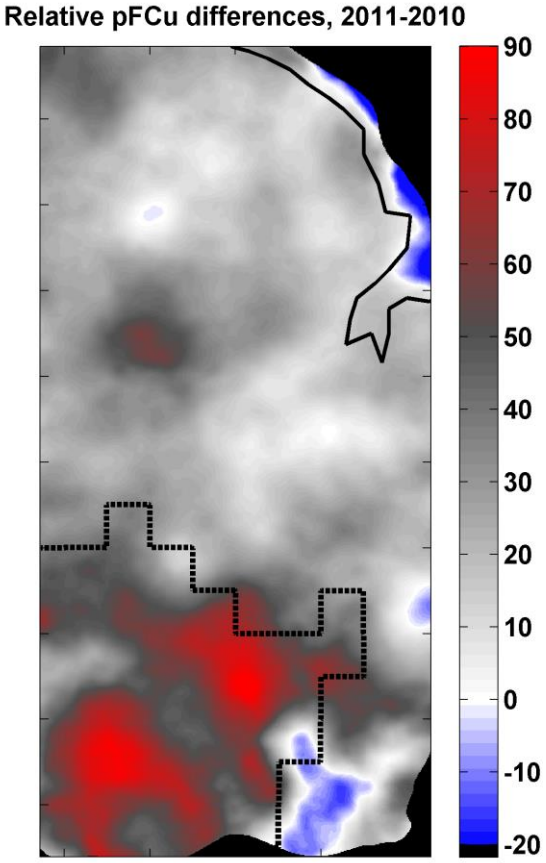

Figure 7. Relative differences (%) in pFCu between 2011 and 2010. Higher probabilities during 2011 (2010) are represented by gray/red (blue) shades. Black dashed line indicates the high 2010 AOD region in Fig. 6. The largest relative changes (up to 90%) occur in the region of high AOD. Areas with $\overline{pFCu} < 0.03$ *are discarded.*

3.3. Enhanced Vegetation Index (EVI) effect on Forest Cumulus (FCu) fields

To minimize influences of AOD and meteorology on the data, we limit the current analysis of EVI effects on FCu fields to the NA region, excluding RH>80% areas, during 2011 (area enclosed by dashed black contour, Fig. 6), taken as a representative example. The J-A-S pFCu data (Fig. 3d) was sorted as a function of the mean J-A-S EVI data (Fig. 4b) for forest (blue dots) and non-forest (magenta dots) landcovers separately (see Fig. 8a). Bin statistics are included in the figure legend/caption. For the forest landcover, we see a positive dependence of pFCu on EVI. This dependence is especially strong for the lower EVI values. The increase in pFCu then saturates at a moderate value of about EVI = 0.54. For the non-forest landcover, the dependence of pFCu on EVI is somewhat different. For low EVI values (EVI < 0.48), there is a

strong positive dependence (similar to that seen in forest landcover), but for higher values of EVI > 0.48 there is a clear decrease of pFCu with EVI. It is important to note that for all EVI values, there is a higher chance of observing an FCu field above forest landcover than non-forest landcover.

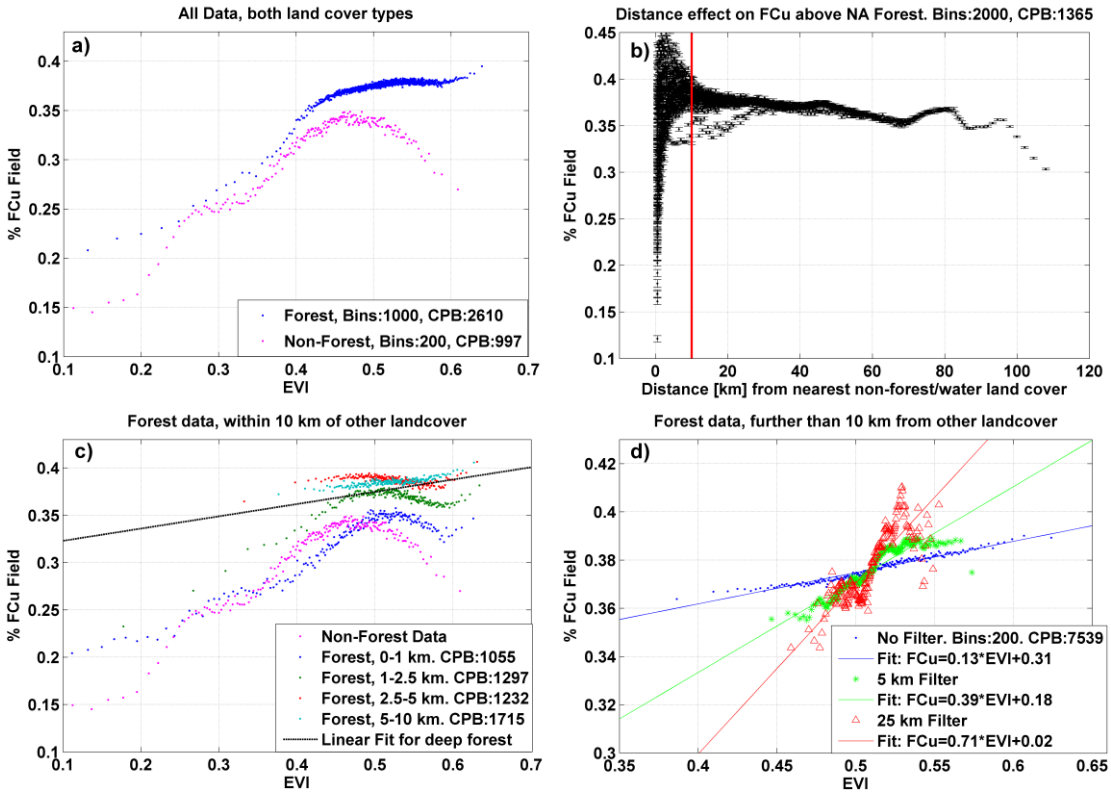

Figure 8. pFCu field as a function of EVI in the NA region (with RH<80%) during J-A-S, 2011. a) All data above forest and non-forest landcover types. Counts per Bin (CPB) included in panel legend. b) pFCu field over forest landcover as a function of distance (km) from nearest non-forest/water landcover pixel. Data corresponds to NA region (with RH<80%). c) Same as (a), but with forest landcover data constrained to within 10 km of other landcover types and sorted into 200 bins. The forest data was divided into four distance from other landcover subsets (see legend) to illustrate the transition from a non-forest-like dependence to a deep-forest-like dependence. Black dashed line is the linear fit for deep forest EVI dependence seen in panel (d). d) Same as (a), but only for forest landcover data further than 10 km from other landcover types. Panel includes raw EVI data (blue), and EVI smoothed with a 5 km (red) or 25 km (green) disk filter. Linear fits for all cases added in panel legend.

Until now, we have focused on limiting the effects of meteorological and aerosol variance on pFCu, but have yet to consider the effects of mesoscale circulations that

393 may form at the boundaries and transition areas between landcover types. Since these
394 circulations are local, their intensity can be represented by the distance from the
395 landcover boundaries. As seen in Fig. 8b for the NA region, pFCu over forest
396 landcover is lowest close to the boundaries with other landcover types, then increases
397 sharply with large variance at short distances (<5km), and is relatively constant at
398 distances larger than ~10 km. The variance seen for distances higher than 80 km may
399 be due to local topography and forest changes. To try and eliminate the mesoscale
400 effects from the EVI analysis, we divided the data into two subsets: i) Forest data
401 within 10 km of other landcover types (Fig. 8c), which we assume includes the bulk
402 of mesoscale circulation effects and ii) Forest data further than 10 km away from
403 other landcover types (Fig. 8d), which we consider to be free of mesoscale circulation
404 effects. There was no point in doing the same exercise for non-forest landcover since
405 more than 95% of that data is closer than 10 km to other landcover types.
406
407 Figures 8c,d illustrate how the pFCu dependence on EVI shifts as we penetrate deeper
408 into the forested areas. In Fig. 8c, forest landcover data was divided to 0-1 km, 1-2.5
409 km, 2.5-5 km, and 5-10 km distance intervals from any other landcover. The non-
410 forest pFCu dependence on EVI from Fig. 8a is added for reference. A gradual
411 transition from a non-forest-like dependence on EVI to a deep-forest-like dependence
412 on EVI (i.e. positive linear, black dashed line in Fig. 8c) is seen. Hence, we can
413 assume that in transition zones between forest landcover and water/non-forest
414 landcovers, a superposition of deep forest and non-forest dependencies on EVI takes
415 place. Generally, for a given EVI value the further the distance from water/non-forest
416 landcovers, the higher the chance of observing FCu fields.
417
418 For deep forest data further than 10 km away from other landcover types (blue dots,
419 Fig. 8d) we can see a positive linear dependence of pFCu on EVI. We applied a linear
420 fit to the data (R^2=0.95, fit details added in figure legend) and obtained a slope
421 of $\frac{\partial(pFCu)}{\partial(EVI)} = 0.13$. Clearly, the well-being and productivity of the deep forest
422 promotes the formation of FCu fields. To test the robustness of the linear trend above
423 (Fig. 8d, blue line), we applied two low-pass disk shaped filters to the EVI data, one
424 with a radius of 5 km (green stars and line, Fig. 8d) and the other with a radius of 25
425 km (red triangles and line, Fig. 8d). Our assumption is that using "smoothed" EVI

data, being less sensitive to local noise, reveals the more robust larger-scale effects of EVI on pFCu. The results of this analysis show that indeed the positive linear trend seen for the deep forest is robust, with stronger dependencies as filter size increases. The slope of pFCu vs. EVI increases to 0.39 for the 5 km filter and 0.71 for the 25 km filter, an increase of 200%, and 450%, respectively. For larger filters with radius > 30 km, the main signal decays because of significant loss of EVI spatial information.

The same process done for 2011 above was repeated for the years 2008-2010. For each year, we took the area with minimum meteorological effect on pFCu (indicated by black dashed contours in Fig. 6), using the methodology described in section 3.1. Areas of high AOD were partially avoided this way as well, although we cannot rule out influence of aerosols on the results for years 2008, 2010 especially. Only deep forest data were considered. The results are summarized in Table. 3. The dependence of pFCu on spatially filtered EVI (only 5 km filter) for 2008-2011 is shown in Fig. 9.

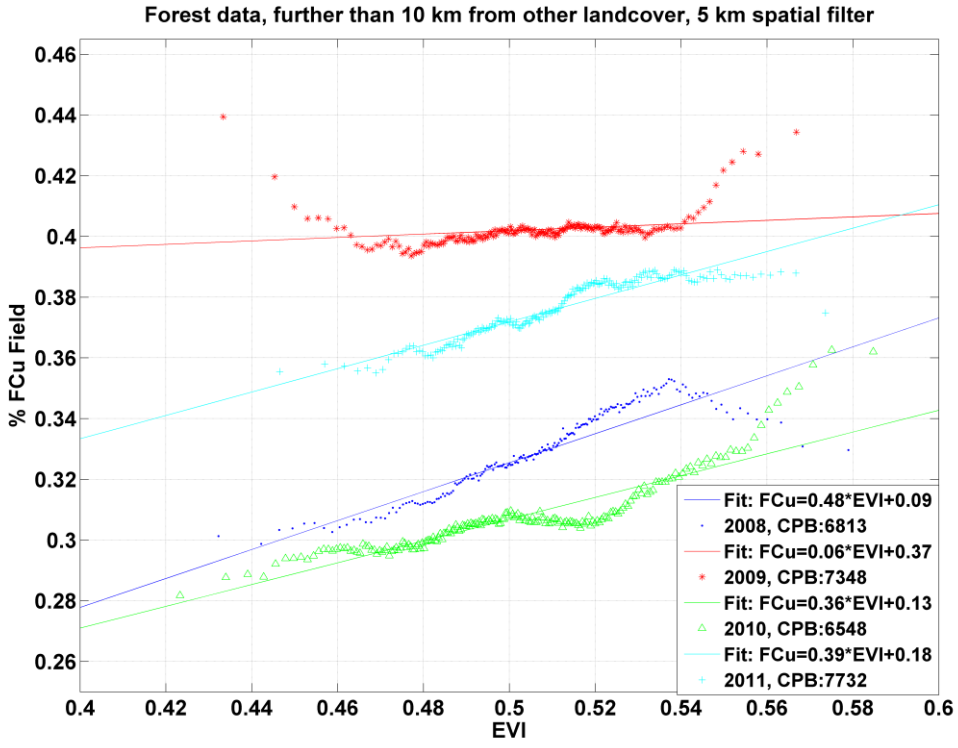

Figure 9. Four year (2008-2011) comparison of pFCu field as a function of EVI, for forest landcover data further than 10 km from other landcover types, and sorted into 200 bins. A 5 km spatial disk filter was applied to the EVI data. Counts per Bin (CPB) and linear fits for all years added in figure legend.

For all years, an increase in pFCu with EVI is seen, yielding positive slopes for all years and spatial filter sizes (Table 3). The minor reductions in pFCu with EVI, seen in Fig. 9 for very high EVI (> 0.55, 2008) or low EVI (< 0.46, 2009), are probably due to local effects and sparse statistics at those EVI ranges. Consistent with 2011, the larger the spatial filter size, the larger the linear fit slope, showing an average increase of more than 200 % for the 5 km filter and 400% for the 25 km filter (Table 3). At the same time, the data become nosier with increasing filter size, reducing the correlation coefficient values from ~ 0.9 without a filter to ~ 0.6 for the 25 km filter. Although consistent with the other years, 2009 shows a much weaker pFCu dependence on EVI. This may be due to the fact that the environmental conditions during that year were especially favorable for FCu formation throughout the domain (see Fig. 6), reducing the second order EVI effect on the clouds.

Table 3. Linear fit statistics for pFCu vs. EVI dependencies using: none, 5 km, 25 km spatial disk filters on the EVI data, for years 2008-2011. Statistics include linear fit slope (a), point of intersection with Y-axis (b), and the R^2 coefficient.

Parameter → **Filter Size (km)↓**	**Year**	$\boldsymbol{a}$	$\boldsymbol{b}$	$\boldsymbol{R^2}$
None	2008	0.23	0.21	0.93
	2009	0.03	0.38	0.33
	2010	0.16	0.22	0.94
	2011	0.13	0.31	0.95
5 km	2008	0.47	0.08	0.84
	2009	0.05	0.37	0.05
	2010	0.35	0.12	0.81
	2011	0.39	0.18	0.87
25 km	2008	0.74	-0.04	0.64
	2009	0.22	0.28	0.14
	2010	0.75	-0.02	0.55
	2011	0.71	0.02	0.74

4. Discussion and Conclusions

In this work we examine the link between the Amazon forest and the clouds that form above it, as part of the effort towards understanding how the anthropogenic forest dilution may affect clouds. By defining Forest Cumulus (FCu) clouds fields, we have created a simple metric that is clearly tightly coupled and highly sensitive to surface changes in the Amazon region. Although chosen subjectively, we note that results of this work are insensitive to changes in the upper and lower thresholds. We tested several sets of threshold ranges and even though the absolute values of pFCu do change, the trends obtained in Sect. 3.3 are the same.

Much of the analyses concentrated on separating first order effects (such as meteorology and biomass burning) from the more subtle second order effect of landcover EVI. Not surprisingly, the meteorological conditions are the main factor that sets the stage for FCu formation. Although the entire study region experiences stable conditions during the dry season, weak meteorological gradients control where FCu fields can form. The South Amazon (SA) subset is usually too dry and stable to enable FCu formation, above forest and non-forest landcover alike. In contrast, the northwestern part and coastal areas of the North Amazon (NA) subset experience relatively unstable conditions which are realized by the increased presence of deep convective clouds and reduction in pFCu. The results in Figs. 6, 7 strengthen previous findings that show that high AOD (i.e. high concentrations of biomass burning aerosol) tends to stabilize the atmosphere and inhibit all types of cloud formation.

Regarding the link between surface EVI and pFCu, five main conclusions can be drawn:

1. FCu fields form exclusively over land areas in the Amazon region, preferably over forest landcover.
2. The chance of observing FCu fields over forest landcover increases with EVI (excluding very low and EVI value ranges for specific years), and can generally be represented by a linear fit.
3. Up to a filter size of 25 km, the pFCu dependence on EVI increases as we increase the spatial smoothing filter size of the EVI data.
4. The chance of observing FCu fields over non-forest landcover increases (decreases) for values lower (higher) than EVI=0.48, and is generally lower than over forest landcover. However, the scattered spatial distribution of non-

forest landcover (see Fig. 4a) and the strong correlation between non-forest EVI and meteorology cast doubt on the significance of this finding.

5. The dependence of pFCu on EVI in transition areas from non-forest/water boundaries into forested landcover can be expressed as a superposition of forest and non-forest dependencies.

These findings show the strong control that landcover and landcover gradients exert on FCu. Even though the dependence need not be linear, EVI can be considered highly correlated with evapotranspiration, implying that high latent heat (moisture) fluxes are crucial for the development and organization of the FCu fields.

Nevertheless, elucidating the dynamical processes which are responsible for the formation of FCu field require future work. We can speculate that the FCu fields correspond to a specific solution of Rayleigh-Benard thermal convection over land (or specifically cloud streets, as discussed in section 1), since the basic physical settings are similar over the Amazon and ocean surfaces, namely: a homogeneous warm surface, and a moist boundary layer with a well defined inversion layer. Hexagonal open convection cells have already been simulated over tropical land in the western pacific (Saito et al., 2001). The fact that vegetation properties control to a large degree both surface fluxes and boundary layer depth (h), and that the Rayleigh number (R_a) is highly dependent on that depth (proportional to h^4), suggests a physical link between forest and the cloud fields formed above.

As for climatic trends in Amazon cloud fields, the effect of large scale biomass burning is more straightforward, with high aerosol loading tending to suppress cloud formation. It is hard to conclude how largescale deforestation would affect total cloud cover since meteorological and landcover gradients roughly coincide in our study region. We can predict a reduction in dry season FCu fields as forest landcover undergoes transition to non-forest or as forest wellbeing decreases (reduction in EVI), however more extensive studies are needed to understand the total effect on the radiation budget and water cycle in the Amazon due to such changes.

Acknowledgements. This research was supported by the European Research Council under the European Union's Seventh Framework Programme (FP7/2007-2013)/ERC (CAPRI, grant # 306965) and by a NASA Interdisciplinary Science (IDS) project managed by H. Maring. We acknowledge the use of Rapid Response imagery (true color images in the work) from the Land Atmosphere Near-real time Capability for EOS (LANCE) system operated by the NASA/GSFC/Earth Science Data and Information System (ESDIS) with funding provided by NASA/HQ. Aerosol Optical Depth (AOD) data and visualizations (Figs. 5 and 6) were produced with the Giovanni online data system, developed and maintained by the NASA GES DISC.

References

Ackerman, S. A., Strabala, K. I., Menzel, W. P., Frey, R. A., Moeller, C. C., and Gumley, L. E.: Discriminating clear sky from clouds with MODIS, J Geophys Res-Atmos, 103, 32141-32157, doi:10.1029/1998jd200032, 1998.

Amante, C., and Eakins, B. W.: ETOPO1 1 Arc-Minute Global Relief Model: Procedures, Data Sources and Analysis, NOAA Technical Memorandum NESDIS NGDC-24, 19, 2009.

Bastable, H. G., Shuttleworth, W. J., Dallarosa, R. L. G., Fisch, G., and Nobre, C. A.: Observations of Climate, Albedo, and Surface Radiation over Cleared and Undisturbed Amazonian Forest, International Journal of Climatology, 13, 783-796, doi:10.1002/joc.3370130706, 1993.

Betts, A. K.: Idealized model for equilibrium boundary layer over land, J Hydrometeorol, 1, 507-523, doi:10.1175/1525-7541(2000)001<0507:Imfebl>2.0.Co;2, 2000.

Betts, A. K.: Land-Surface-Atmosphere Coupling in Observations and Models, J Adv Model Earth Sy, 1, 18, doi:10.3894/James.2009.1.4, 2009.

Brümmer, B.: Roll and cell convection in wintertime arctic cold-air outbreaks, J Atmos Sci, 56, 2613-2636, doi:10.1175/1520-0469(1999)056<2613:RACCIW>2.0.CO;2, 1999.

Chagnon, F. J. F., Bras, R. L., and Wang, J.: Climatic shift in patterns of shallow clouds over the Amazon, Geophysical Research Letters, 31, L24212, doi:10.1029/2004gl021188, 2004.

565 Cutrim, E., Martin, D. W., and Rabin, R.: Enhancement of Cumulus Clouds over
566 Deforested Lands in Amazonia, Bulletin of the American Meteorological Society, 76,
567 1801-1805, doi:10.1175/1520-0477(1995)076<1801:Eoccod>2.0.Co;2, 1995.
568 Davidi, A., Koren, I., and Remer, L.: Direct measurements of the effect of biomass
569 burning over the Amazon on the atmospheric temperature profile, Atmos Chem Phys,
570 9, 8211-8221, doi:10.5194/acp-9-8211-2009, 2009.
571 Figueroa, S. N., and Nobre, C. A.: Precipitation distribution over central and western
572 tropical South America, Climanalise, 5, 36-45, 1990.
573 Fisch, G., Culf, A. D., and Nobre, C. A.: Modelling convective boundary layer growth
574 in Rondonia, in: Amazonian Deforestation and Climate, edited by: Gash, J. H. C.,
575 Nobre, C. A., Roberts, J. M., and Victoria, R. L., John Wiley & Sons, Chichester, UK,
576 425–436, 1996.
577 Fisch, G., Tota, J., Machado, L. A. T., Dias, M. A. F. S., Lyra, R. F. D., Nobre, C. A.,
578 Dolman, A. J., and Gash, J. H. C.: The convective boundary layer over pasture and
579 forest in Amazonia, Theor Appl Climatol, 78, 47-59, doi:10.1007/s00704-004-0043-
580 x, 2004.
581 Friedl, M. A., Sulla-Menashe, D., Tan, B., Schneider, A., Ramankutty, N., Sibley, A.,
582 and Huang, X. M.: MODIS Collection 5 global land cover: Algorithm refinements
583 and characterization of new datasets, Remote Sensing of Environment, 114, 168-182,
584 doi:10.1016/j.rse.2009.08.016, 2010.
585 Glenn, E. P., Huete, A. R., Nagler, P. L., and Nelson, S. G.: Relationship between
586 remotely-sensed vegetation indices, canopy attributes and plant physiological
587 processes: What vegetation indices can and cannot tell us about the landscape,
588 Sensors-Basel, 8, 2136-2160, doi:10.3390/S8042136, 2008.
589 Glenn, E. P., Nagler, P. L., and Huete, A. R.: Vegetation Index Methods for
590 Estimating Evapotranspiration by Remote Sensing, Surv Geophys, 31, 531-555,
591 doi:10.1007/s10712-010-9102-2, 2010.
592 Hansen, M., DeFries, R., Townshend, J. R., and Sohlberg, R.: Global land cover
593 classification at 1 km spatial resolution using a classification tree approach,
594 International Journal of Remote Sensing, 21, 1331-1364,
595 doi:10.1080/014311600210209, 2000.
596 Heiblum, R. H., Koren, I., and Altaratz, O.: Analyzing coastal precipitation using
597 TRMM observations, Atmos Chem Phys, 11, 13201-13217, doi:10.5194/acp-11-
598 13201-2011, 2011.

599 Huete, A., Didan, K., Miura, T., Rodriguez, E. P., Gao, X., and Ferreira, L. G.:
600 Overview of the radiometric and biophysical performance of the MODIS vegetation
601 indices, Remote Sensing of Environment, 83, 195-213, doi:10.1016/S0034-
602 4257(02)00096-2, 2002.
603 Koren, I., Kaufman, Y. J., Remer, L. A., and Martins, J. V.: Measurement of the
604 effect of Amazon smoke on inhibition of cloud formation, Science, 303, 1342-1345,
605 doi:10.1126/science.1089424, 2004.
606 Koren, I., Martins, J. V., Remer, L. A., and Afargan, H.: Smoke invigoration versus
607 inhibition of clouds over the Amazon, Science, 321, 946-949,
608 doi:10.1126/science.1159185, 2008.
609 Lewis, S. L., Brando, P. M., Phillips, O. L., van der Heijden, G. M., and Nepstad, D.:
610 The 2010 Amazon drought, Science, 331, 554, doi:10.1126/science.1200807, 2011.
611 Malda, D., Vilà-Guerau de Arellano, J., van den Berg, W. D., and Zuurendonk, I. W.:
612 The role of atmospheric boundary layer-surface interactions on the development of
613 coastal fronts, Ann. Geophys., 25, 341-360, doi:10.5194/angeo-25-341-2007, 2007.
614 Martins, J. V., Tanre, D., Remer, L., Kaufman, Y., Mattoo, S., and Levy, R.: MODIS
615 Cloud screening for remote sensing of aerosols over oceans using spatial variability,
616 Geophysical Research Letters, 29, 8009, doi:10.1029/2001gl013252, 2002.
617 Mu, Q., Heinsch, F. A., Zhao, M., and Running, S. W.: Development of a global
618 evapotranspiration algorithm based on MODIS and global meteorology data, Remote
619 Sensing of Environment, 111, 519-536, doi:10.1016/j.rse.2007.04.015, 2007.
620 Nagler, P. L., Scott, R. L., Westenburg, C., Cleverly, J. R., Glenn, E. P., and Huete,
621 A. R.: Evapotranspiration on western US rivers estimated using the Enhanced
622 Vegetation Index from MODIS and data from eddy covariance and Bowen ratio flux
623 towers, Remote Sensing of Environment, 97, 337-351, doi:10.1016/j.rse.2005.05.011,
624 2005.
625 Nair, U. S., Lawton, R. O., Welch, R. M., and Pielke Sr, R. A.: Impact of land use on
626 Costa Rican tropical montane cloud forests: Sensitivity of orographic cloud formation
627 to deforestation in the plains, Journal of geophysical research, 111, D02108,
628 doi:10.1029/2005JD006096, 2003.
629 Nobre, C. A., Mattos, L. F., Dereczynski, C. P., Tarasova, T. A., and Trosnikov, I. V.:
630 Overview of atmospheric conditions during the Smoke, Clouds, and Radiation -
631 Brazil (SCAR-B) field experiment, J Geophys Res-Atmos, 103, 31809-31820,
632 doi:10.1029/98jd00992, 1998.

633 Parrish, D. F., and Derber, J. C.: The National Meteorological Center's spectral
634 statistical-interpolation analysis system, Monthly Weather Review, 120, 1747-1763,
635 doi:10.1175/1520-0493(1992)120<1747:TNMCSS>2.0.CO;2, 1992.
636 Pielke Sr, R. A., Pitman, A., Niyogi, D., Mahmood, R., McAlpine, C., Hossain, F.,
637 Goldewijk, K. K., Nair, U., Betts, R., and Fall, S.: Land use/land cover changes and
638 climate: modeling analysis and observational evidence, Wiley Interdisciplinary
639 Reviews: Climate Change, 2, 828-850, doi:10.1002/wcc.144, 2011.
640 Rabin, R. M., Stadler, S., Wetzel, P. J., Stensrud, D. J., and Gregory, M.: Observed
641 Effects of Landscape Variability on Convective Clouds, Bulletin of the American
642 Meteorological Society, 71, 272-280, doi:10.1175/1520-
643 0477(1990)071<0272:Oeolvo>2.0.Co;2, 1990.
644 Ramos da Silva, R., Gandu, A. W., Sá, L. D. A., and Silva Dias, M. A. F.: Cloud
645 streets and land–water interactions in the Amazon, Biogeochemistry, 105, 201-211,
646 doi:10.1007/s10533-011-9580-4, 2011.
647 Ray, D. K., Nair, U. S., Welch, R. M., Han, Q. Y., Zeng, J., Su, W. Y., Kikuchi, T.,
648 and Lyons, T. J.: Effects of land use in Southwest Australia: 1. Observations of
649 cumulus cloudiness and energy fluxes, J Geophys Res-Atmos, 108, 4414,
650 doi:10.1029/2002jd002654, 2003.
651 Remer, L. A., Kaufman, Y. J., Tanre, D., Mattoo, S., Chu, D. A., Martins, J. V., Li, R.
652 R., Ichoku, C., Levy, R. C., Kleidman, R. G., Eck, T. F., Vermote, E., and Holben, B.
653 N.: The MODIS aerosol algorithm, products, and validation, J Atmos Sci, 62, 947-
654 973, doi:10.1175/Jas3385.1, 2005.
655 Running, S. W., Justice, C. O., Salomonson, V., Hall, D., Barker, J., Kaufmann, Y. J.,
656 Strahler, A. H., Huete, A. R., Muller, J. P., Vanderbilt, V., Wan, Z. M., Teillet, P., and
657 Carneggie, D.: Terrestrial Remote-Sensing Science and Algorithms Planned for Eos
658 Modis, International Journal of Remote Sensing, 15, 3587-3620,
659 doi:10.1080/01431169408954346, 1994.
660 Saha, S., Nadiga, S., Thiaw, C., Wang, J., Wang, W., Zhang, Q., Van den Dool, H.
661 M., Pan, H. L., Moorthi, S., Behringer, D., Stokes, D., Pena, M., Lord, S., White, G.,
662 Ebisuzaki, W., Peng, P., and Xie, P.: The NCEP Climate Forecast System, Journal of
663 Climate, 19, 3483-3517, doi:10.1175/Jcli3812.1, 2006.
664 Saito, K., Keenan, T., Holland, G., and Puri, K.: Numerical Simulation of the Diurnal
665 Evolution of Tropical Island Convection over the Maritime Continent, Monthly

Weather Review, 129, 378-400, doi:10.1175/1520-0493(2001)129<0378:NSOTDE>2.0.CO;2, 2001.

Salomonson, V. V., Barnes, W. L., Maymon, P. W., Montgomery, H. E., and Ostrow, H.: Modis - Advanced Facility Instrument for Studies of the Earth as a System, Ieee T Geosci Remote, 27, 145-153, doi:10.1109/36.20292, 1989.

Souza, E. P., Renno, N. O., and Dias, M. A. F. S.: Convective circulations induced by surface heterogeneities, J Atmos Sci, 57, 2915-2922, doi:10.1175/1520-0469(2000)057<2915:Ccibsh>2.0.Co;2, 2000.

Ten Hoeve, J., Remer, L., Correia, A., and Jacobson, M.: Recent shift from forest to savanna burning in the Amazon Basin observed by satellite, Environmental Research Letters, 7, 024020, doi:10.1088/1748-9326/7/2/024020, 2012.

Wang, J., Chagnon, F. J., Williams, E. R., Betts, A. K., Renno, N. O., Machado, L. A., Bisht, G., Knox, R., and Bras, R. L.: Impact of deforestation in the Amazon basin on cloud climatology, Proceedings of the National Academy of Sciences of the United States of America, 106, 3670-3674, doi:10.1073/pnas.0810156106, 2009.

Xiao, X. M., Braswell, B., Zhang, Q. Y., Boles, S., Frolking, S., and Moore, B.: Sensitivity of vegetation indices to atmospheric aerosols: continental-scale observations in Northern Asia, Remote Sensing of Environment, 84, 385-392, doi:10.1016/S0034-4257(02)00129-3, 2003.